**Figure S1.** Upper panel: phase function of dust aerosols calculated for the Algeria case at the peak of the dust injection and 120 min after the peak at the wavelength of 3, 6, 10, and 15 µm. Lower panel: calculated scattering-to-absorption ratio as a function of the wavelength as seen by the FTIR. Calculations have been performed by subtracting from the total integrated scattering the fraction towards the forward direction, which enters the FTIR detector and is not measured as extinction. The fraction that enters the FTIR has been calculated by taking into account the geometry of the instrument and the dust size, and it is larger than 50-70% at all wavelengths considered. Uncertainties in the scattering-to-absorption ratio are calculated with the error propagation formula taking into account the uncertainty in the size distribution. The obtained scattering-to-absorption ratio indicates that scattering is predominant at 3 µm, also mostly due to the fact that absorption is close to zero at this wavelength, then above 6 µm it represents on average less than 10% of the absorption signal. Thus, we can reasonably assume that above 6 µm the FTIR spectrum represents dust absorption.

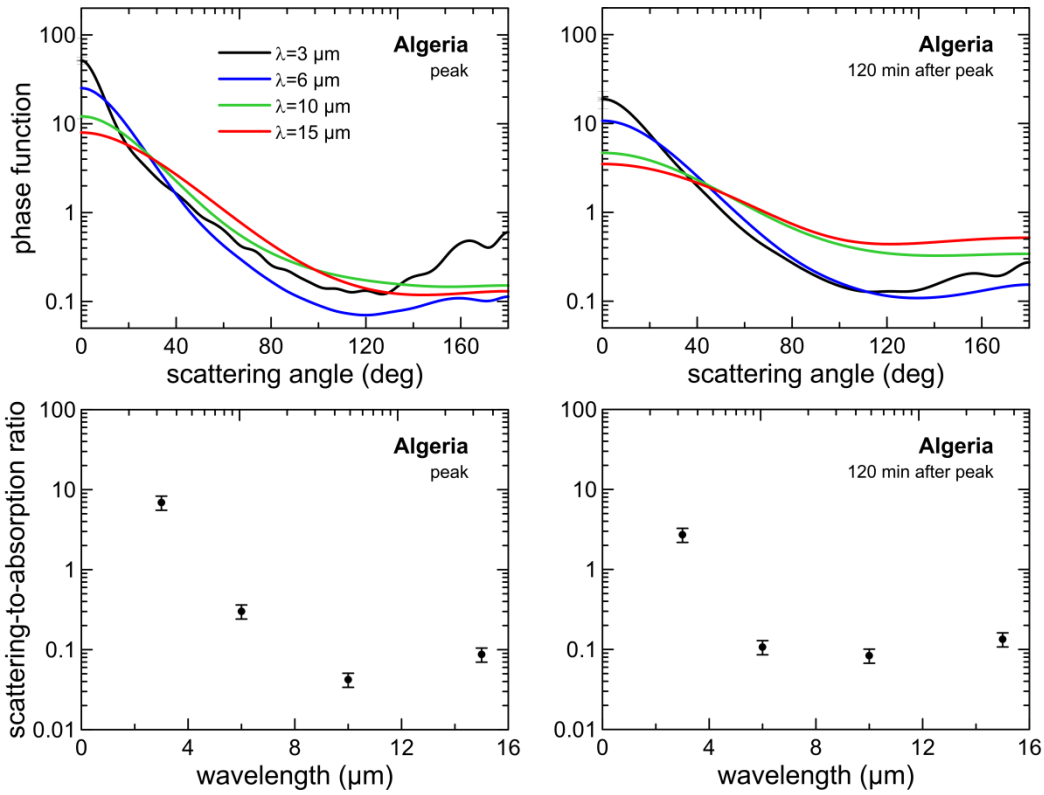

**Figure S2.** Emission spectrum of the WELAS white light source (Xenon arc lamp 35 W) measured with a LI-COR LI-1800.

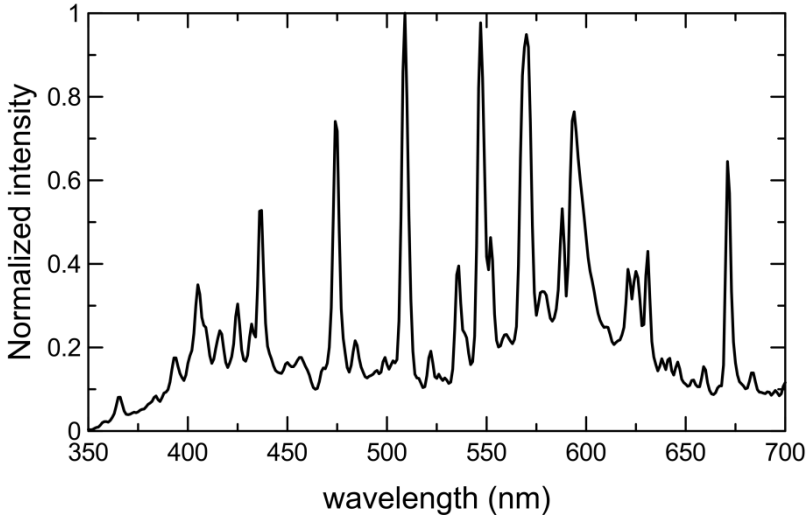

**Figure S3.** Comparison of the size distribution for the different instruments. Measurements from the SMPS ($D_g$=0.1-0.3 µm), the SkyGrimm ($D_g$=0.3-1.0 µm), and the WELAS ($D_g$>1.0 µm) at 30 min after the peak of the injection for the Algeria and Atacama cases are shown. Error bars indicate the 10-min standard deviation for the SMPS and the SkyGrimm, and the combination of standard deviation and $L_{WELAS}$ ($D_g$) uncertainty for the WELAS. Error bars that extend to negative numbers on the log scale have been omitted for clarity. The interpolation curve at $D_g$>8 µm is also reported in the plot.

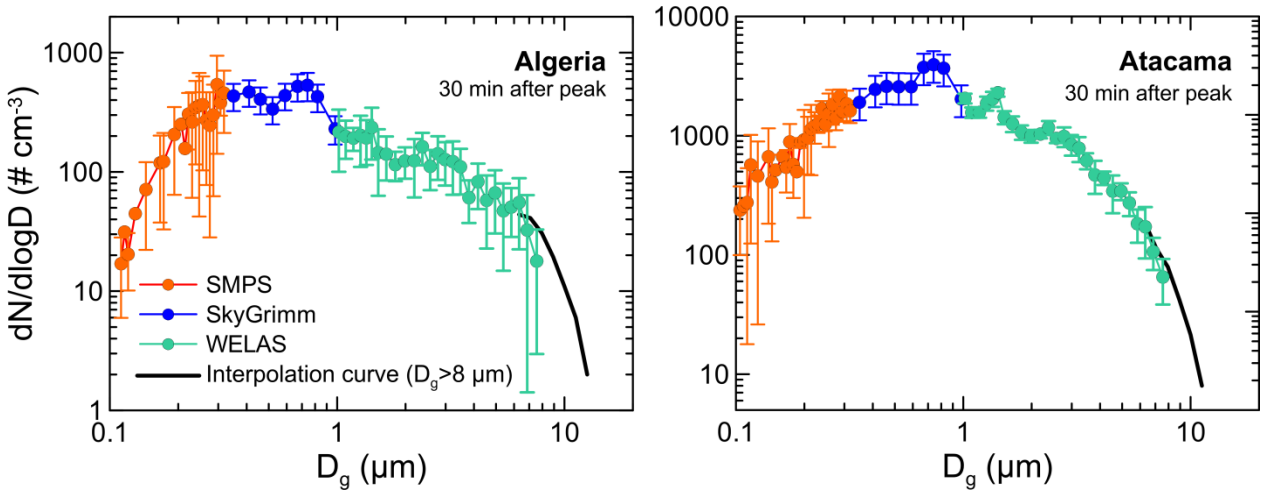

**Figure S4.** Comparison of the size distribution within the CESAM chamber (labelled as FTIR) and at the input of the sampling filter system measured at 30 min after the peak of the injection for the Algeria case.

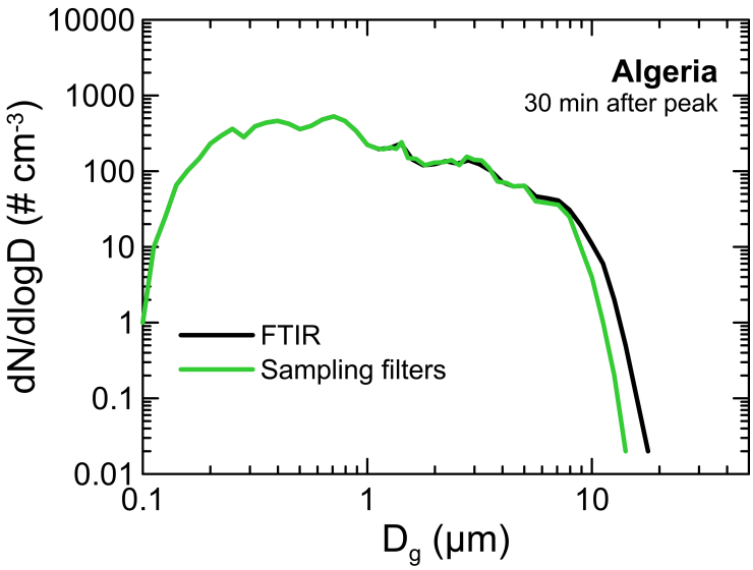

**Figure S5.** Number distribution ($dN/dlogD_g$, bottom panel), mass distribution ($dM/dlogD_g$ center panel), and total mass concentration (top panel) measured in CESAM during the experiment with Arizona dust.

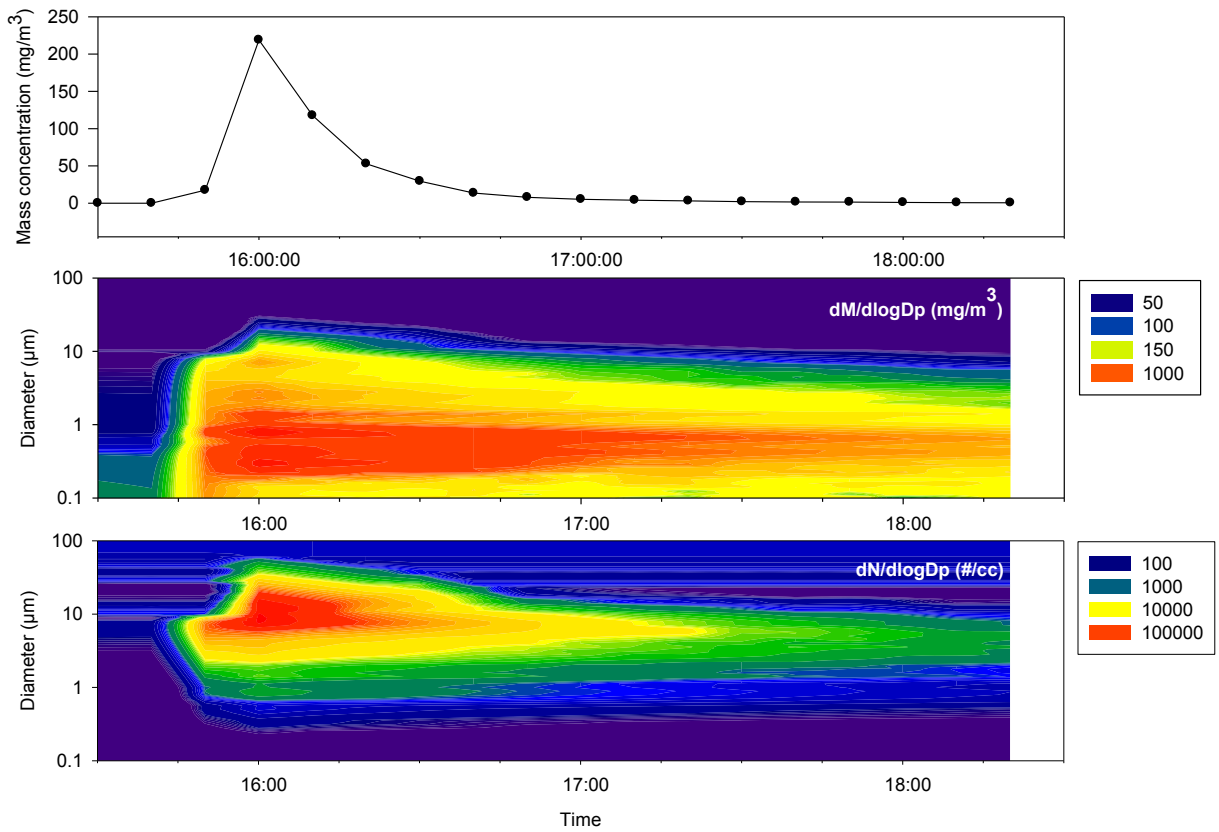


**Table S1.** Calibration coefficients by mineral, obtained from the calibration of the diffractometer used in this study. The origin of the standard minerals is reported. The calibration coefficients ($K_i$) represent the slope of the linear fit between the number of diffracted counts by unit mass. The correlation coefficient $R^2$ of the fit for each mineral is also reported.

| **Mineral** | **Origin** | **$K_i$ (cps mg$^{-1}$)** | **$R^2$** |
|---|---|---|---|
| Quartz | Fontainebleau, France | 2874 ± 272 | 0.80 |
| Orthoclase | Galerie des mineraux de Paris, France | 2850 ± 389 | 0.69 |
| Albite | Ontario, Canada | 1271 ± 108 | 0.98 |
| Calcite | Bédarieux, France | 2288 ± 242 | 0.99 |
| Dolomite | Traversella, Italy | 2945 ± 276 | 0.99 |
| Gypsum | Unknown | 1053 ± 189 | 0.99 |